



# Late Quaternary incision rates in the Vésubie catchment area (Southern French Alps) from in situ-produced $^{36}\text{Cl}$ cosmogenic nuclide dating: Tectonic and climatic implications

Marianne Saillard, Carole Petit, Yann Rolland, Regis Braucher, Didier Bourles, Swann Zerathe, Marie Revel, Anthony Jourdon

## ► To cite this version:

Marianne Saillard, Carole Petit, Yann Rolland, Regis Braucher, Didier Bourles, et al.. Late Quaternary incision rates in the Vésubie catchment area (Southern French Alps) from in situ-produced  $^{36}\text{Cl}$  cosmogenic nuclide dating: Tectonic and climatic implications. *Journal of Geophysical Research: Earth Surface*, 2014, 119 (5), pp.1121 - 1135. 10.1002/2013JF002985 . hal-01708833

**HAL Id: hal-01708833**

**<https://hal.science/hal-01708833>**

Submitted on 12 Nov 2021

**HAL** is a multi-disciplinary open access archive for the deposit and dissemination of scientific research documents, whether they are published or not. The documents may come from teaching and research institutions in France or abroad, or from public or private research centers.

L'archive ouverte pluridisciplinaire **HAL**, est destinée au dépôt et à la diffusion de documents scientifiques de niveau recherche, publiés ou non, émanant des établissements d'enseignement et de recherche français ou étrangers, des laboratoires publics ou privés.

Copyright

## RESEARCH ARTICLE

10.1002/2013JF002985

## Key Points:

- We obtained fifteen  $^{36}\text{Cl}$  exposure ages of a polished river cliff
- An incision rate of 2.2 mm/a is computed for the last 15 ka
- Incision rates are related to Holocene climatic changes

## Correspondence to:

C. Petit,  
petit@geoazur.unice.fr

## Citation:

Saillard, M., C. Petit, Y. Rolland, R. Braucher, D. L. Bourlès, S. Zerathe, M. Revel, and A. Jourdon (2014), Late Quaternary incision rates in the Vésubie catchment area (Southern French Alps) from in situ-produced  $^{36}\text{Cl}$  cosmogenic nuclide dating: Tectonic and climatic implications, *J. Geophys. Res. Earth Surf.*, 119, 1121–1135, doi:10.1002/2013JF002985.

Received 24 SEP 2013

Accepted 16 APR 2014

Accepted article online 23 APR 2014

Published online 27 MAY 2014

Late Quaternary incision rates in the Vésubie catchment area (Southern French Alps) from in situ-produced  $^{36}\text{Cl}$  cosmogenic nuclide dating: Tectonic and climatic implications

Marianne Saillard<sup>1</sup>, Carole Petit<sup>1</sup>, Yann Rolland<sup>1</sup>, Régis Braucher<sup>2</sup>, Didier L. Bourlès<sup>2</sup>, Swann Zerathe<sup>1</sup>, Marie Revel<sup>1</sup>, and Anthony Jourdon<sup>1</sup>
<sup>1</sup>Géoazur, Université de Nice Sophia-Antipolis, CNRS, Observatoire de la Côte d'Azur, Valbonne, France, <sup>2</sup>Aix-Marseille Université, CNRS-IRD-Collège de France, UM 34 CEREGE, Technopôle de l'Environnement Arbois-Méditerranée, Aix-en-Provence, France

**Abstract** We have estimated recent river incision rates using the in situ-produced  $^{36}\text{Cl}$  cosmogenic nuclide concentrations. The target site consists of a ~25 m high vertical profile along a polished river cliff located in Jurassic limestones in the Vésubie catchment area, in the southern French Alps. The  $^{36}\text{Cl}$  exposure ages of the sampled river polished surface range from 3 to 14 ka, i.e., after the Last Glacial Maximum. Our data suggest as a first approximation a linear age/height relationship and lead to a mean incision rate of 2.2 mm a<sup>-1</sup> over the last 14 ka. More precisely, incision rates are characterized by two peaks reaching ~2 and 4–5 mm a<sup>-1</sup> at 4–5 ka and 11–12 ka, respectively, separated by a period experiencing a lower incision rate (~1 mm a<sup>-1</sup>). A chi-plot of the river longitudinal profile suggests that on the long term, the river is close to equilibrium conditions with a concavity index of 0.475. The evolution of the Vésubie River longitudinal profile over a time period of 2 Ma based on the stream power law of river incision was then modeled with varying erodibility coefficients and uplift rates ranging from 0.5 to 2 mm a<sup>-1</sup>. The best fitting models yield erodibility coefficient values ranging from 2.5 to 9.0 × 10<sup>-6</sup> m<sup>-0.475</sup> a<sup>-1</sup> for the considered uplift rates. For long-term uplift rates lower than 2 mm a<sup>-1</sup>, an increase of the erodibility coefficient during the last 16 ka, with two peaks at 11–12 and 4–5 ka, is necessary to precisely match the observed incision rates and is interpreted as resulting from recent climatic changes. These variations do not strongly affect the general shape of the river profile and suggest that the measured short-term incision rate is dominated by a climatic signal, which does not preclude the possible role of tectonic uplift.

## 1. Introduction

River incision is a complex process governed both by external factors such as climate, lithology, tectonic, or isostatic uplift, and by internal adjustments of the river dynamics [e.g., Attal *et al.*, 2008; Daniels, 2008; Vandenberghe, 2003]. At a given location along the river channel, incision rate may thus vary through time depending on the amount of water runoff (mainly controlled by climatic conditions), transient effects due to localized channel uplift or base-level fall (i.e., knickpoint retreat), or autogenic factors. Determination of river incision rates at different time scales has many applications, either for short-term soil denudation issues, nutrient fluxes variations, or climate changes estimates [e.g., Ferrier *et al.*, 2013, and references therein]. It is also widely used to understand the internal dynamics of a river system and its response to various external forcings [e.g., Brocard *et al.*, 2003]. Finally, from a tectonic point of view, river incision may help deciphering rock uplift patterns in actively uplifting mountain ranges [e.g., Wobus *et al.*, 2006; Kirby and Whipple, 2012; Baotian *et al.*, 2013]. Accurate measurements of river incision rates coupled with reliable climatic estimates can thus help decipher the role of external forcing like tectonics or isostatic movements, and understanding the internal behavior of the catchment system. However, short time scale (i.e., one or several years) measurements of river incision can be difficult to extrapolate to long time scales, due to the stochastic behavior of large erosive events such as floods [e.g., Stock *et al.*, 2004] and to the variability of denudation processes during glacial and interglacial cycles. Therefore, isolating a single parameter like tectonic uplift rates from measured river incision rates is not a straightforward issue. Classically, tectonic geomorphology aims at quantifying tectonic rates from offset recent markers such as terraces, and/or from the dynamic response of fluvial systems (i.e., incision rate variations) or hillslope processes to vertical motions. For instance, over the two last decades, cosmogenic

nuclides such as  $^{10}\text{Be}$  have been widely used to date fluvial terrace abandonment ages and infer Quaternary slip rates on various active faults [e.g., Brown *et al.*, 1998; Ritz *et al.*, 1995; Van der Woerd *et al.*, 1998] or to date the onset of landslide activity [e.g., Sanchez *et al.*, 2010] or individual rock avalanches [Akçar *et al.*, 2012]. Besides, dating of strath terraces can also be used to determine river incision rates and infer denudation rates [e.g., Burbank *et al.*, 1996]. In any case, deriving uplift rates or incision rates from staircase terraces rely on the implicit assumption that the exposure age corresponds to the age of terrace abandonment and that incision started immediately after. Furthermore, one has to determine whether the terrace formation is due to dominant tectonic or climatic forcing [e.g., Baotian *et al.*, 2013].

Here we propose an original alternative method to quantify long-term river incision rates, in order to identify both climatic and tectonic controls on the river system evolution. We provide an accurate determination of the duration of exposure to cosmic rays of well-preserved characteristic markers of river incision such as river cliffs or gorges using their accumulated in situ-produced  $^{36}\text{Cl}$  cosmogenic nuclide concentrations [Schaller *et al.*, 2005; Richter *et al.*, 2010].

A first attempt of dating bedrock gorge incision has been recently carried out using in situ-produced  $^{10}\text{Be}$  on a limited number of samples (4–5 per site) due to difficult sampling conditions [Valla *et al.*, 2010]. Up to now, the  $^{36}\text{Cl}$  method has been mainly applied to the dating of successive exposures of an exhumed normal fault escarpment during repeated earthquakes [Benedetti *et al.*, 2002, 2003; Palumbo *et al.*, 2004; Carcaillet *et al.*, 2008; Schlagenhauf *et al.*, 2010], revealing that high-resolution denudation rate estimates could be determined with this method. In all cases, an important issue regarding the dating of surface features using in situ-produced cosmogenic nuclides is the difficulty to accurately estimate the amount of nuclides that has been accumulated before either the surface deposition or the surface exposure of the collected samples. Accurate determination of bedrock surface exposure duration necessitates estimating these “inherited”  $^{10}\text{Be}$  or  $^{36}\text{Cl}$  concentrations, which affect the age of the following exposure event [Sadier *et al.*, 2012]. In addition, denudation processes (e.g., rock falls and dissolution) affecting the bedrock surface may impact the age estimate when integrated over long time period ( $> 30$  ka), but are generally negligible otherwise. However, both the effects of inherited cosmogenic nuclides and hillslope denudation may be considered as negligible for river cliffs for which the topographic shielding is large, and providing that the sampled polished surfaces are well preserved.

Following an approach similar to that of Schaller *et al.* [2005] and Richter *et al.* [2010], this paper provides quantitative data on medium-term (i.e., several ka) river incision rates using in situ-produced  $^{36}\text{Cl}$  cosmogenic nuclide concentrations in a river gorge (Vésubie River, Southern French Alps). It relies on 15 samples from a ~25 m high river cliff, insuring a satisfying resolution on incision rate estimates. The results are then combined with a simple model of river incision to infer the relative importance of local uplift rates and recent climatic variations on the river incision rate over the last 15 ka. We then discuss these results in light of the geodynamic and climatic contexts of the Southern French Alps and make the connection between the active deformation of the Alps and the neighboring Ligurian margin.

## 2. Geological and Tectonic Setting

The Vésubie River is a large tributary of the Var River, which is the largest catchment in the southern French Alps (about 2200 km<sup>2</sup>). The Vésubie River flows in an approximately NS direction, from the external crystalline Argentera-Mercantour massif down to its confluence with the Var River, about 40 km away from its source, and then to the Mediterranean Sea (Figure 1). The Vésubie River source is located in crystalline rocks in the Argentera-Mercantour massif, but the river cuts through the Mesozoic and Cenozoic cover of the southernmost subalpine belts along most of its course. These belts have been deformed mostly during the Miocene during the opening of the Ligurian basin and the alpine collision [e.g., Clauzon, 1975; Campredon *et al.*, 1977; Sage *et al.*, 2011]. This area is still undergoing active deformation as evidenced by the abundant, although moderate seismicity [e.g., Courboulex *et al.*, 2007; Bauve *et al.*, 2012, 2014; Petersen *et al.*, 2014]. Several pieces of evidence advocate for ongoing uplift of the margin: submarine canyons located east of the Var river mouth display a convex-up longitudinal profile characteristic of recent or active uplift on a fault system located offshore, at the foot of the thinned continental margin [Migeon *et al.*, 2011], and the Messinian erosion surface visible on seismic profiles appears deformed and tilted [Bigot-Cormier *et al.*, 2004]. However, indices of recent uplift are much more difficult to detect onshore. Corsini *et al.* [2004] and Sanchez *et al.* [2011] propose an onset of the exhumation of the Argentera-Mercantour massif in early Miocene times (~22 Ma)

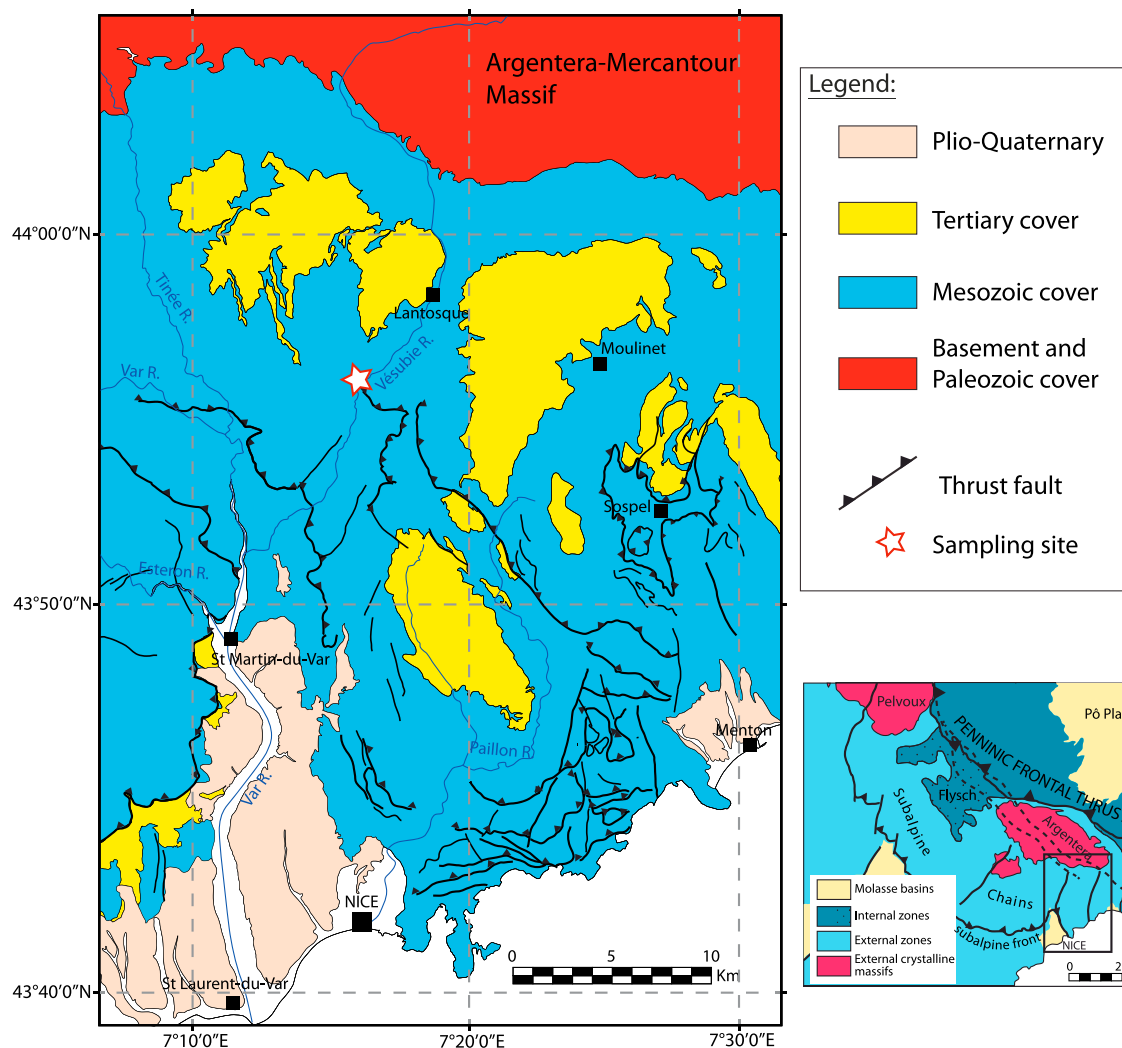


**Figure 1.** Geologic setting of the Vésubie and Var catchment areas. Southern French Alps [after Sanchez *et al.*, 2011]. Open red star shows the sample location. Inset shows the tectonic setting of the study area in the framework of the western Alps. Internal units consist of alpine metamorphic domains thrust over the external, nonmetamorphic basement and cover units.

from  $^{39}\text{Ar}/^{40}\text{Ar}$  dating on phengites. Besides these results, there was until now no available data on the rate of river incision in the sediment cover, i.e., between the crystalline basement outcropping to the north and the submarine part of the margin to the south.

To quantify river incision, a nicely preserved polished river cliff located in Upper Jurassic (Tithonian) limestones in the Vésubie catchment area (Southern French Alps) was targeted. This cliff has been cut almost vertically by the Vésubie stream and is located about 10 km upstream from its confluence with the Var River (Figure 2). This site has several advantages: the polished gorge is overhanging, and it is particularly well preserved and devoid of any trace of erosion, dissolution, or collapse. Some calcite stalactites appear on the cliff surface, due to the resurgence at the top of the cliff of highly concentrated karstic waters, which suggests that water runoff on the cliff surface cannot cause additional dissolution and is localized on these concretions. Because of the sedimentary strata dip, only the right bank of the river exhibits such a cliff, the gentler slope of the left bank insuring thus a sufficient exposure to cosmic rays. The lithology is homogeneous, which guarantees that possible incision rate variations are actually due to climatic or tectonic changes, and not to lithological contrasts. Finally, the site is located in the lower part of the Vésubie stream at an altitude of about 300 m, far away from any imprint of glacial erosion, which are limited to elevations of more than 1500 m [Julian, 1980]. At this place, the valley has the shape of a typical wineglass canyon with an



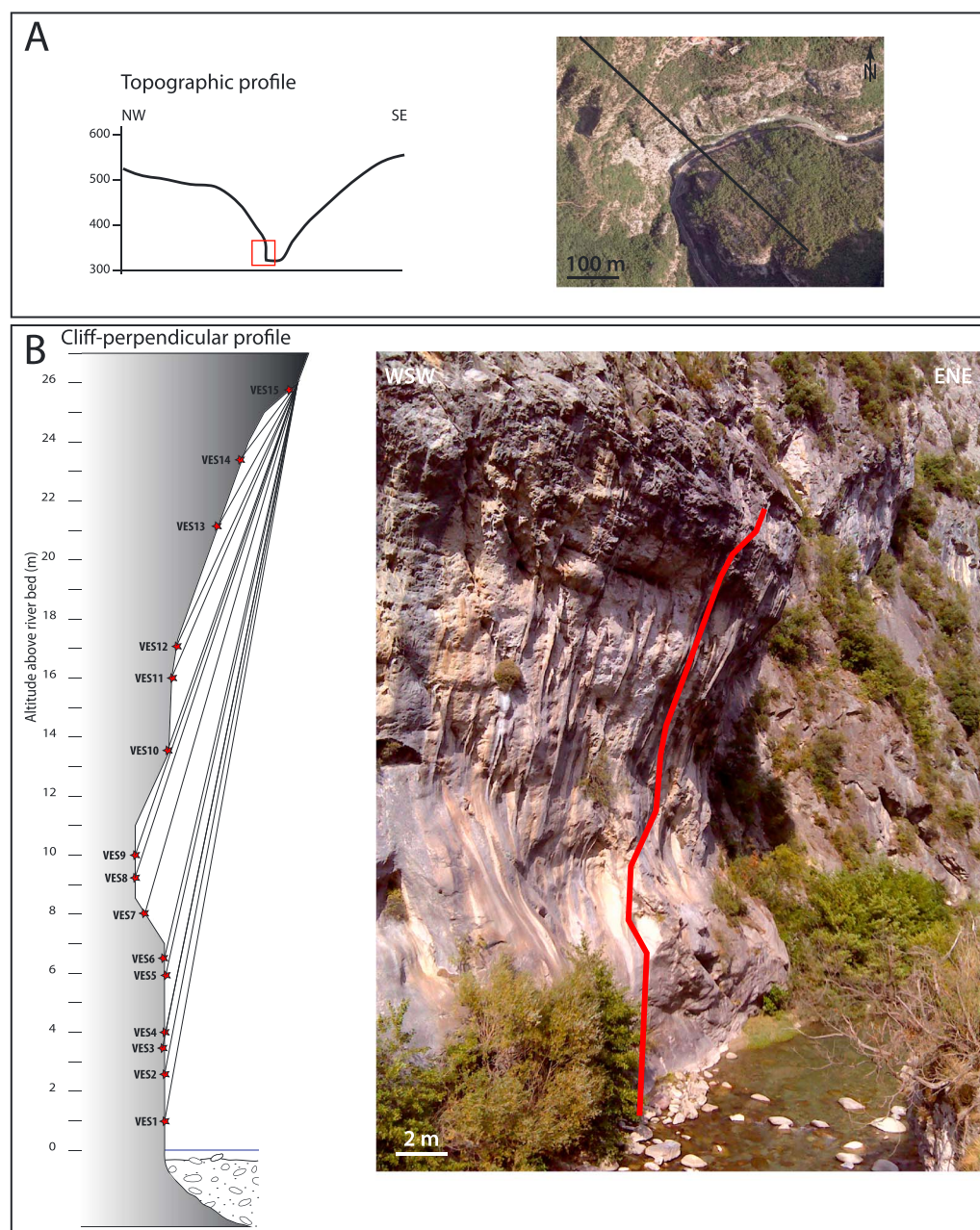


**Figure 2.** (a) Valley-perpendicular topographic profile and aerial view of the sampling site. Open red rectangle corresponds to the close-up view shown below. (b, left) Cliff-perpendicular topographic profile with altitudes relative to the present river bed. Red stars show the samples location. Thin lines are used to calculate the shielding effect of the overhanging cliff. Sample names are indicated in bold. (b, right) Picture of the polished river cliff. Red line indicates the approximate position of the sampled vertical profile.

ancient V-shaped alluvial valley located ~30 m above the river bed, and underlain by an almost vertical gorge (Figure 2a). Therefore, the effect of subglacial erosion can be ruled out.

### 3. Sampling and Methods

#### 3.1. Chlorine-36 Sampling and Dating

Fifteen samples were collected along the cliff using a hammer and chisel. Their latitude, altitude, and position along the profile were precisely determined in the field (Table 1 and Figure 2b). The samples were crushed,

**Table 1.** Field Information and Scaling Factors Used for Calculation of the Production Rates<sup>a</sup>

Sample	Altitude Above Sea Level (m)	Height Above River Bed (m)	Cliff Slope (°)	Shielding Factor $S_f$	Scaling Factor Spallation $S_n$	Scaling Factor Muons $S_\mu$
VES1	327	1	99	0.392	1.315	1.126
VES2	328.6	2.6	99	0.392	1.317	1.127
VES3	329.4	3.4	100	0.388	1.318	1.127
VES4	329.7	3.7	101	0.381	1.318	1.127
VES5	331.7	5.7	101.5	0.381	1.320	1.128
VES6	332.4	6.4	102	0.379	1.321	1.129
VES7	333.9	7.9	105.5	0.362	1.329	1.129
VES8	335.2	9.2	107	0.349	1.324	1.130
VES9	336	10	107	0.349	1.325	1.131
VES10	339.6	13.6	109	0.335	1.330	1.133
VES11	342	16	111	0.320	1.332	1.134
VES12	342.9	16.9	113	0.304	1.333	1.134
VES13	347.2	21.2	118	0.260	1.339	1.137
VES14	349.4	23.4	124	0.205	1.341	1.138
VES15	351.5	25.5	110	0.327	1.344	1.139

<sup>a</sup>Sample coordinates are 43°56'06.7"N and 7°15'54.8"E. No erosion or cover correction is applied. Sample thickness is 5 cm.

sieved, and chemically prepared at the French Cosmogenic Nuclides National Laboratory (LN2C; Centre Européen de Recherche et d'Enseignement de Géosciences de l'Environnement (CEREGE), Aix-en-Provence) to precipitate AgCl following the procedure fully described in *Schimmelpfennig et al.* [2009]. Their  $^{36}\text{Cl}$  and Cl concentrations were determined by isotope dilution accelerator mass spectrometry at the French accelerator mass spectrometry (AMS) national facility Atmosphere-Surface Turbulent Exchange Research ASTER (CEREGE, Aix-en-Provence) and were both normalized to a  $^{36}\text{Cl}$  standard prepared by K. Nishiizumi: KNSTD1600 with a given  $^{36}\text{Cl}/^{35}\text{Cl}$  value of  $(2.11 \pm 0.06) \times 10^{-12}$  [Sharma et al., 1990; Fifield et al., 1990]. The decay constant of  $2.303 \pm 0.016 \times 10^{-6} \text{ a}^{-1}$  used corresponds to a  $^{36}\text{Cl}$  half-life ( $T_{1/2}$ ) of  $3.014 \times 10^5$  years. All the analytical and chemical data are presented with respect to the recommendations of *Dunai and Stuart* [2009]. Analytical uncertainties include the counting statistics, machine stability, and blanks correction ( $^{36}\text{Cl}/^{35}\text{Cl}$  blank ratios are 0.75 and  $3.87 \times 10^{-15}$ ). Blank corrections represent between 0.6 and 6.7% of the sample concentrations. Cl concentrations of the samples are ranging from 15 to 32 ppm.

The full chemical composition of three samples was analyzed by inductively coupled plasma–atomic emission spectroscopy (ICP–AES) and inductively coupled plasma–mass spectrometry (ICP–MS) at the Centre de Recherches Péetrographiques et Géochimiques - Service d'Analyse des Roches et des Minéraux (CRPG–SARM) facility (Nancy, France) in order to insure that the chemical composition of the limestone was homogeneous, which appears to be the case (Table 2). All the contributions from the various  $^{36}\text{Cl}$  production mechanisms using these relevant parameters were then taken into account to determine each sample specific production rate [Schimmelpfennig et al., 2009]. The in situ-produced  $^{36}\text{Cl}$  production rate also depends on the incoming cosmic ray flux that varies with the Earth magnetic field, with the latitude of the study area and with the amount of topographic obstruction around the sample, the latter being generally the most important factor to take into account to obtain an accurate age estimate [Gosse and Phillips, 2001]. Because temporal geomagnetic field variations are negligible at these latitudes and over the period considered, the latitudinal and altitudinal scaling were determined at a constant geomagnetic field [Stone, 2000]. The elementary  $^{36}\text{Cl}$  production rate from spallation of calcium at sea level and high latitude used is  $42 \pm 2.0$  atoms of  $^{36}\text{Cl} \text{ g}^{-1}$  of  $\text{Ca} \text{ a}^{-1}$  as established at a site less than a few hundreds of kilometer away from the sampling site [Braucher et al., 2011]. Calibrated at a site for which latitude, elevation, and exposure duration are similar to those of the sampling site, this “local” production rate significantly reduces the uncertainties linked to the scaling processes. Finally, in our case, considering the topographic shielding was particularly important because the samples were collected on an almost vertical, even sometimes overhanging surface, which means that at least 50% of the incoming ray flux was blocked by the topography in the immediate vicinity of the samples. In order to insure a correct estimate of the topographic shielding, we have measured both the local (i.e., near the sample location) and the average cliff slope above the sample (Figure 2b and Table 1). Measurements were performed directly at the sampling sites using a compass, inclinometer, and a tape measure. The largest number (angles larger than 90° indicate an overhanging

**Table 2.** Major and Trace Element Composition of Three Samples VES4, VES12, and VES15 Measured by ICP-AES and ICP-MS, Respectively, at the SARM-CRPG Facility (Nancy, France)<sup>a</sup>

Sample	SiO <sub>2</sub> (wt %)	Al <sub>2</sub> O <sub>3</sub> (wt %)	Fe <sub>2</sub> O <sub>3</sub> (wt %)	MnO (wt %)	MgO (wt %)	CaO (wt %)	Na <sub>2</sub> O (wt %)	K <sub>2</sub> O (wt %)	TiO <sub>2</sub> (wt %)	P <sub>2</sub> O <sub>5</sub> (wt %)	H <sub>2</sub> O (%)	CO <sub>2</sub> (%)	Li (ppm)	B (ppm)	Cl (ppm)	Cr (ppm)	Gd (ppm)	Sm (ppm)	Th (ppm)	U (ppm)
Uncertainties	< 15%	< 15%	< 15%	< 10%	< 10%	< 2%	< 15%	< 15%	< 15%	< 10%	< 10%	< 5%	< 15%	< 15%	< 15%	< 15%	< 15%	< 15%	< 15%	< 15%
VES4	0.34	0.13	0.09	0.0068	0.57	54.04	0.02	0.03	< d.t.	0.04	0.29	43.83	1.4	2	33	< d.t.	0.645	0.513	0.29	0.56
VES12	0.38	0.14	0.06	0.0077	0.48	54.27	0.02	0.03	< d.t.	0.04	0.38	43.68	1.0	2	< 20	< d.t.	0.564	0.440	0.25	0.53
VES15	0.81	0.2	0.08	0.0081	0.48	54.2	0.04	0.05	< d.t.	0.03	0.31	43.43	1.2	2	23	< d.t.	0.623	0.510	0.58	0.94

<sup>a</sup> d.t. means detection threshold.

surface) was then used for the shielding estimate due to the cliff obstruction. Besides the cliff itself, the shielding effect of the surrounding topography was measured with a compass as the height (in degrees) of the horizon with respect to the horizontal. The topographic shielding factor  $S_f$  is then as follows:

$$S_f = \int_{\phi=0}^{2\pi} \int_{\theta=\theta_h}^{\pi/2} \sin^{2.3}\theta \cos\theta d\theta d\phi - \int_{\phi=0}^{\phi_c} \int_{\theta=\theta'_h}^{\pi/2} \sin^{2.3}\theta \cos\theta d\theta d\phi \quad (1)$$

where  $\theta$  is the angle of incidence of cosmic rays measured from the horizontal,  $\theta_h$  is the angle of topographic obstruction for a “normal” (i.e., not overhanging) surface,  $\phi$  is the azimuth,  $\phi_c$  is the azimuthal extent of the overhanging cliff (about 180°) and  $\theta'_h$  is the supplementary angle of topographic obstruction for an overhanging surface ( $\theta'_h = \pi - \theta$ ). Shielding factors range from 0.20 for the most shielded samples to 0.40 for the most exposed ones (Table 1). Measurement error of the topographic obstruction of about 5° will induce shielding factor estimate uncertainties ranging from less than 0.4% (for a low dipping topography) to at most 5% (for large topographic angles). Moreover, the shielding between sampled points varies only with the local dip of the cliff (i.e., on an azimuth aperture of less than 180°). Consequently, such shielding factor estimate errors will introduce a systematic bias, which will affect absolute age values but will have a very limited effect on age differences, hence on the incision rate estimates.

The exposure ages were finally calculated according to *Schimmelpenninck et al.* [2009]. Because the sampled bedrock is highly shielded and deep beneath from the overlying surface topography, the inherited component has been neglected. The presented exposure ages are thus maximum, yielding to potentially underestimated incision rates. Given the reasons presented above, the age bias due to possible inherited <sup>36</sup>Cl is most likely negligible and anyway systematic; hence, it does not affect the incision rate estimates.

### 3.2. Numerical Model of River Incision

Inferring uplift rates from incision rates would require the Vesubie River to be globally in an equilibrium state, i.e., that river incision everywhere balances a possible tectonic uplift or base-level fall. Incision is often modeled using the stream power law [e.g., *Stock and Montgomery*, 1999; *Whipple and Tucker*, 1999, and references therein]:

$$E = KA^m S^n \quad (2)$$

where  $E$  is the incision rate,  $K$  is an erodibility coefficient,  $A$  is the drainage area,  $S$  is the along-channel slope, and  $m$  and  $n$  are area and slope coefficients, respectively. For an equilibrium river profile, the incision rate  $E$  balances the relative uplift rate  $U$  such as  $E = U$  and

$$S = \left(\frac{U}{K}\right)^{1/n} A^{-m/n} \quad (3)$$

where the ratio  $m/n$  is the concavity index.

Slope-area relationships can therefore be used to infer an equilibrium or transient state of river incision. However, as pointed out by *Perron and Royden* [2013], slope-area plots are often scattered because of the topographic noise. Therefore, we chose to use the chi-plot method of *Perron and Royden* [2013] to assess equilibrium conditions along the Vesubie River. The chi-plot method is based on the transformation of the linear  $x$  coordinate system (i.e., the river longitudinal distance) into a nonlinear dimensionless coordinate system which accounts for the power law growth of the drainage area with the

**Table 3.** Natural Chlorine, Calcium, and Cosmogenic  $^{36}\text{Cl}$  Content in the Limestone Samples and Resulting  $^{36}\text{Cl}$  Exposure Ages<sup>a</sup>

Sample	Cl (ppm)	Ca (wt %)	$^{36}\text{Cl}/^{35}\text{Cl}$ ( $10^{-14}$ )	Atoms $^{36}\text{Cl}/\text{g}$	Atoms $^{36}\text{Cl}/\text{g}$ Uncertainty	$^{36}\text{Cl}$ Age (yr)	Internal Uncertainty (year)
VES1	25.93	38.6	4.0723	$32.939\text{E}^3$	2872.8	3100	265
VES2	25.43	39.7	3.5559	$40.786\text{E}^3$	2636.5	3961	255
VES3	24.04	39.5	5.6413	$42.605\text{E}^3$	2738.6	4105	256
VES4	27.87	39.9	4.2001	$50.003\text{E}^3$	3082.3	4929	304
VES5	22.59	39.9	6.4384	$72.085\text{E}^3$	3894.9	7329	396
VES6	23.61	38.5	7.5541	$56.008\text{E}^3$	5699.0	5564	560
VES7	24.53	39.8	5.9445	$69.699\text{E}^3$	4151.0	7417	442
VES8	23.89	39.9	7.8241	$91.989\text{E}^3$	4367.8	10219	485
VES9	21.96	39.8	11.1803	$83.041\text{E}^3$	8704.2	9056	942
VES10	20.06	39.3	12.4060	$87.755\text{E}^3$	4163.6	10017	458
VES11	32.11	39.1	8.9020	$75.790\text{E}^3$	4562.0	8688	502
VES12	15.05	39.7	6.0929	$62.310\text{E}^3$	3365.7	8098	437
VES13	21.88	39.8	6.5153	$83.226\text{E}^3$	4669.6	12387	695
VES14	20.88	39.7	7.5460	$83.430\text{E}^3$	3928.0	15876	747
VES15	19.99	40.0	10.1884	$113.482\text{E}^3$	4586.9	13435	543

<sup>a</sup>To compare the  $^{36}\text{Cl}$  exposure ages presented in this paper with ages issued from different dating methods. A 4.76% uncertainty related to the spallation production rate has to be added to the internal uncertainties. Spallation production rate is  $42 \pm 2.0$  atoms of  $^{36}\text{Cl}$   $\text{g}^{-1}$  of  $\text{Ca}$   $\text{a}^{-1}$ . The samples contain between  $1.8$  and  $6.8 \times 10^6$  atoms of  $^{36}\text{Cl}$ , and between  $1.14$  and  $4.26 \times 10^{19}$  atoms of  $\text{Cl}$ .

downstream distance. The chi-coordinate integrates drainage area variations (with respect to a reference area  $A_0$ ) over the stream distance from its base-level position  $x_b$  up to the considered channel point  $x$ :

$$\chi = \int_{x_b}^x \left( \frac{A_0}{A'x} \right)^{m/n} dx \quad (4)$$

Within this coordinate system, an equilibrium river profile in a landscape experiencing uniform uplift and with uniform rock resistance to erosion approaches a straight line, providing that  $m$  and  $n$  are correctly determined. However, a straight line profile on a chi-plot does not necessarily mean that the river is in steady state. If this is the case, the slope of the regression line  $C$  can then be used to either infer the uplift rate or the erodibility coefficient with the following:

$$C = \left( \frac{U}{K} \right)^{1/n} A_0^{-m/n} \quad (5)$$

To assess equilibrium and estimate the  $m/n$  ratio of the Vésudie River profile, we use the chi-analysis tools software developed by Mudd *et al.* [2014] with a reference drainage area of  $1000 \text{ m}^2$ . We then model the evolution of the incision in the Vésudie River over a time period of 2 Ma (i.e., long enough to get close to dynamic equilibrium conditions). The model is based on the stream power law of river incision (see above) and assumes that the drainage area does not change with time. The latter is measured along the river using a digital elevation model extracted from the SRTM (Shuttle Radar Topography Mission) 90 m resolution data set. The model computes iteratively the effect of river incision and uplift: at each time step, the slope is modified depending on the uplift rate, which in turn affects the local incision rate. We test the respective effects of uplift rate and erodibility coefficient  $K$  in order to fit the observed river longitudinal profile. The location of the channel point where uplift occurs is located close to the mouth of the Var River, i.e., about 80 km downstream from the Vésudie source, which means that all the landscape above sea level is uplifted. We assume that the uplift rate does not change with time during the whole model duration. Sea level variations are approximated by periodic high level stands every  $\sim 110$  ka followed by progressive sea level drops until the Last Glacial Maximum (LGM) when the Mediterranean sea level reached about 120 m below sea level [Lambeck and Bard, 2000]. Initial conditions consist of a concave equilibrium profile located 100 to 300 m higher than the present-day one. Our tests show that the long-term equilibrium river longitudinal profile is not sensitive to initial conditions.

We then compute an age/height relationship at the channel location corresponding to the sample site (40 km downstream of the river head) such as the following:

$$h(t) = \int_{t=0}^{^{36}\text{Cl}_{\text{age}}} E dt \quad (6)$$



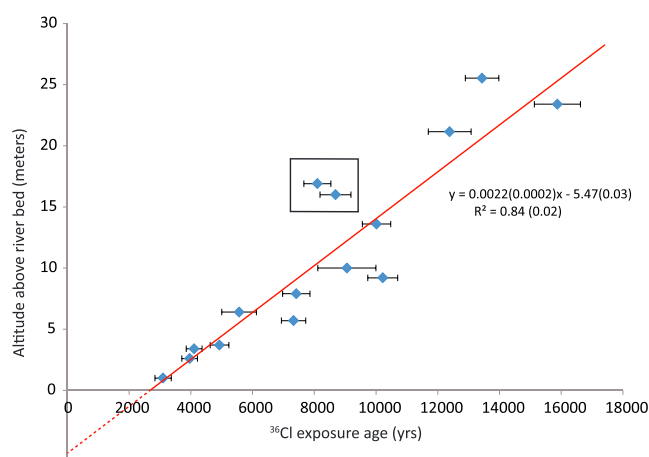


**Figure 3.** Altitude (relative to the river bed) and  $^{36}\text{Cl}$  exposure ages of the 15 date samples with estimated uncertainties. Box indicates two inferred outliers (VES11 and VES12). Solid line is computed from a linear regression (excluding the two outliers) and gives a mean incision rate of  $2.2 \text{ mm a}^{-1}$ . Numbers in parenthesis correspond to estimated uncertainties on the linear regression fit.

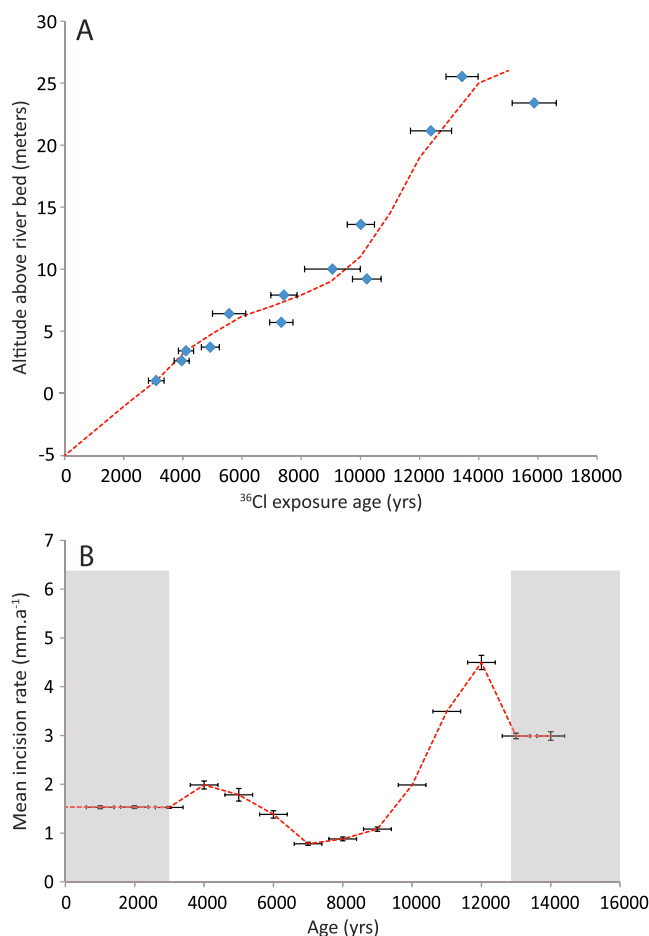


**Figure 4.** (a) Mean  $^{36}\text{Cl}$  ages and (b) incision rates computed with a sliding average window of 1 ka (dashed red lines). Grey areas correspond to under-constrained incision rates due to too few data points.

where  $h(t)$  is the height of a sample above the actual river bed (where  $h = 0$ ),  $E$  is the incision rate, and  $t$  is the time since the beginning of the model. As  $h$  is only a relative altitude, we choose as a pinpoint the maximum altitude of the river cliff, i.e., 26 m for an age of circa 16 ka, extrapolated from the dated samples (section 4). We then modify the  $K$  value for the last 16 ka in order to fit the observed age/height distribution.

## 4. Results

### 4.1. Chlorine-36 Exposure Ages and Incision Rates

The  $^{36}\text{Cl}$  exposure ages of the sampled polished surface range from 3 to 14 ka (Table 3 and Figure 3), i.e., posterior to the LGM phase ( $\sim 20$  ka). Although the expected increase of the sample ages with the height above the river bed is globally observed, samples VES11 and VES12 appear to be much younger than expected considering their altitude and are therefore possible outliers. A linear trend fits well the data, giving a mean incision rate of  $2.2 \pm 0.2 \text{ mm a}^{-1}$  for the last 14 ka (Figure 3). The best fitting regression line (computed without the two supposed outliers) implies a y intercept roughly 5 m below the actual river bed, which is possibly due to the transient natural infill by boulders and pebbles visible in the river bed (Figure 2). In order to evaluate more precisely incision rate variations and limit the biases inherent to data noise, mean incision rates were computed from a smoothed age/height curve obtained by sliding averaging windows of 1 ka (Figure 4a). Incision rates are characterized by two peaks reaching  $\sim 2$  and  $4\text{--}5 \text{ mm a}^{-1}$  at  $4\text{--}5$  ka and  $11\text{--}12$  ka, respectively (Figure 4b), separated by a period of lower incision rate ( $\sim 1 \text{ mm a}^{-1}$ ).

### 4.2. Chi-Plot and Forward Model of River Incision

The best fit regression line in the chi-plot is found for the Vésubie River with  $m/n = 0.475$  (Figure 5 (top)). In the following, we will assume that  $m = 0.475$

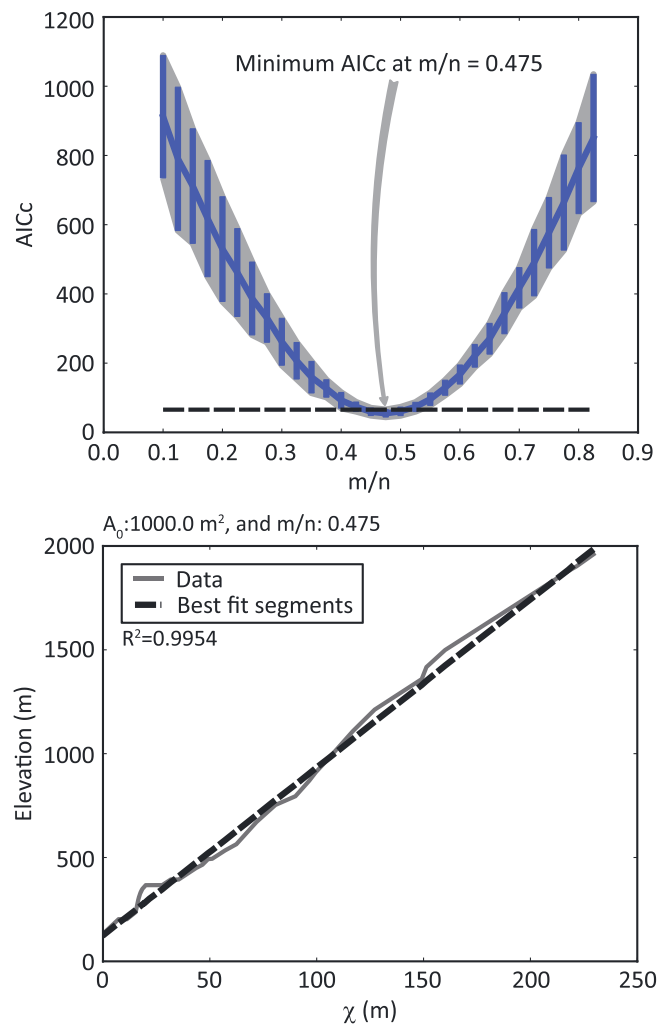


**Figure 5.** (top) Akaike Information Criterion [Akaike, 1974] calculated by the chi-analysis tool [Mudd et al., 2014] to estimate the goodness of fit as a function of the concavity index ( $m/n$ ) in the chi-plot representation of Perron and Royden [2013]. (bottom) Chi-plot of the Vésubie River longitudinal profile with the best fitting  $m/n$  value (0.475).

and  $n = 1$ , which is consistent with the stream power law in which the rate of incision is proportional to the rate of energy dissipation per unit bed area [e.g., Whipple and Tucker, 1999]. The computed  $R^2$  value is very close to 1 ( $R^2 = 0.9954$ , Figure 5 (bottom)), which suggests that the river has a typical concave up longitudinal profile with a concavity index of 0.475. Although minor deviations from this profile occur, possibly due to local effects (e.g., changes in substrate) or short-term variations in boundary conditions (e.g., climate), the river longitudinal profile possibly represents a long-term equilibrium profile. A first set of models is then performed in order to test the effect of uplift rate  $U$  and erodibility coefficient  $K$  on the shape of the equilibrium river profile (Figure 6a). Based on short- and long-term uplift rate estimates published in the study area [Serpelloni et al., 2013; Sanchez et al., 2011; Darnault et al., 2012], we test  $U$  values between 0.5 and 2 mm a<sup>-1</sup>. We then define a best fitting  $K$  value that allows us to obtain a river equilibrium profile matching the observed one for these uplift rates (Figure 6a and Table 4). However, without any other constraints, it is impossible to determine  $U$  and  $K$  independently. This long-term model is then used to fix a pinpoint that corresponds to the maximum height of the river cliff slightly extrapolated from dated sample ages and heights,

i.e., approximately 26 m above the river bed for an estimated age of ~16 ka. We then test if long-term  $U/K$  couples matching the river longitudinal profile also satisfyingly explain the observed age/height distribution of dated samples on the river cliff (Figure 6b). For all uplift rates lower than 2 mm a<sup>-1</sup> (i.e., lower than the recent incision rate), the long-term  $U/K$  values predict incision rates that are too small for the recent period. Considering that the uplift rate should not significantly vary in the short-term, we then change the average  $K$  value for the last 16 ka in order to fit the observed age/height distribution. Results show that over the last 16 ka, the  $K$  value should be of  $9 \pm 1 \times 10^{-6} \text{ m}^{-0.475} \text{ a}^{-1}$  for every tested uplift rate, in order to fit the observations.

We then use this average  $K$  estimate with an arbitrary uplift rate of 1 mm a<sup>-1</sup>, and take into account higher frequency variations of the  $K$  coefficient over the last 16 ka in order to fit more precisely the obtained ages, heights and incision rates. Short-term and high-amplitude variations of the erodibility coefficient  $K$  during the last 16 ka allow us to match precisely the observed ages and incision rates but do not strongly affect the general equilibrium profile of the river (Figure 7). The largest erodibility coefficient is modeled for the time period between 11 and 12 ka, where it becomes more than twice as high as the average 16 ka value (i.e.,  $\sim 2 \times 10^{-5} \text{ m}^{-0.475} \text{ a}^{-1}$ ).

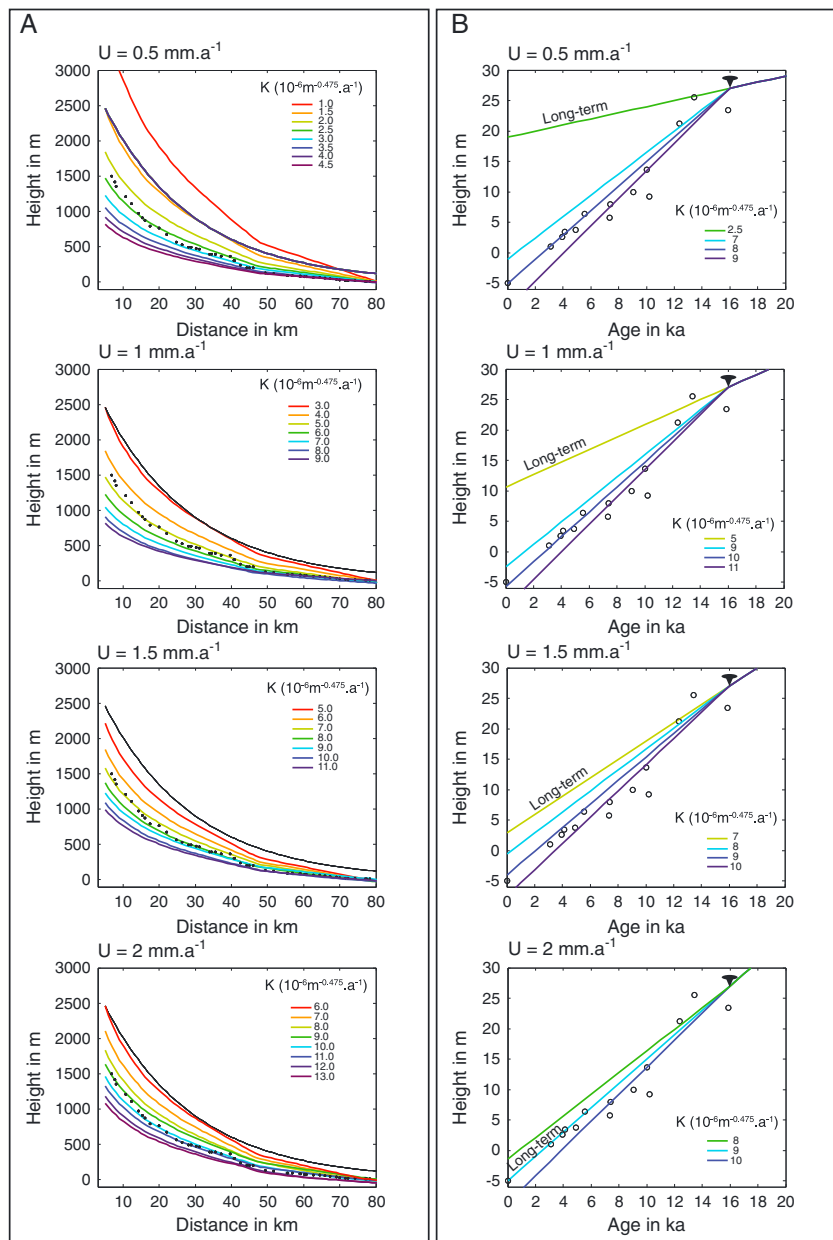


**Figure 6.** (a) Models of the equilibrium river profile (colored lines) with different  $K$  values for four different long-term uplift rates of 0.5 to 2 mm a<sup>-1</sup>. Solid dots are measured altitudes along the river channel based on the SRTM digital elevation model. (b) Age/height relationships predicted at the sampling site for different long-term uplift rates and average short-term (16 ka)  $K$  values, including the long-term ones (best fitting curve on the corresponding Figure 6a). Open dots correspond to measured sample ages. Pinpoint at 16 ka, 26 m is indicated. Note that for every uplift rate lower than 2 mm a<sup>-1</sup>, the average short-term (16 ka)  $K$  value is larger than the long-term one.

**Table 4.** Best Fitting  $K$  Values for Different Long-Term Uplift Rates Based on the Modeling of the River Longitudinal Profile

Uplift Rate (mm a <sup>-1</sup> )	$K$ (m <sup>-0.475</sup> a <sup>-1</sup> )
0.5	$2.5 \times 10^{-6} \pm 0.5 \times 10^{-6}$
1.0	$5 \times 10^{-6} \pm 0.5 \times 10^{-6}$
1.5	$7 \times 10^{-6} \pm 0.5 \times 10^{-6}$
2.0	$9 \times 10^{-6} \pm 1.0 \times 10^{-6}$

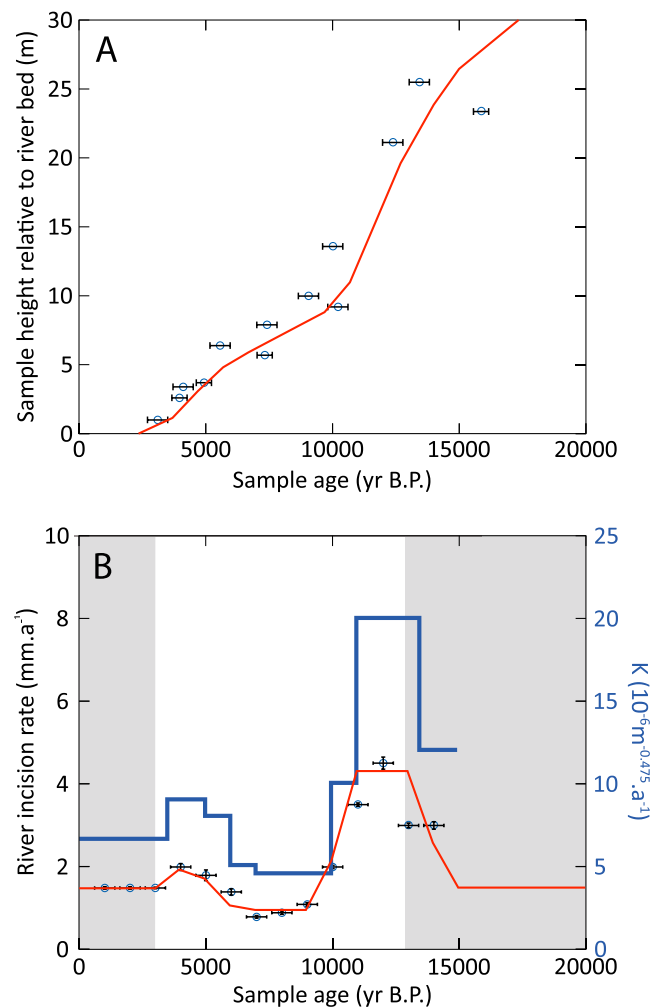


**Figure 7.** (a) Measured (open blue dots) and modeled (red line) height and age of the samples with short-term variations of the  $K$  coefficient. (b) Computed and modeled river incision rate through the last 16 ka. Thick blue line indicates the value of the  $K$  coefficient (scale on the right side of the plot).

recognize two different glacial stages, which they attributed to the Marine Isotopic Stages MIS-6 and MIS-2. Unfortunately, the chronology of glacier retreat and related climatic and environmental changes over the last 20,000 years, and particularly before 14 ka, is poorly constrained in alpine lakes on the French side of the massif [De Beaulieu, 1977; Jorda and de Beaulieu, 1977; Jorda and Rosique, 1994; Jorda et al., 2000]. However, in upper valley slopes, polished surfaces have been dated by the  $^{10}\text{Be}$  cosmogenic nuclide at  $14.9 \pm 0.8$  ka [Darnault et al., 2012], constraining the chronology of the deglaciation at these altitudes during the oldest Dryas, that is, well after the LGM period constrained by Federici et al. [2012] at  $20 \pm 1$  ka. Furthermore, cosmogenic  $^{10}\text{Be}$  dating of most glacier-polished surfaces at 11–12 ka indicates that deglaciation occurred in two stages at circa 15 and 11 ka in the Argentera-Mercantour Massif [Darnault et al., 2012] and was locally correlated with an important release of glacial sediments and an increased river flow. The enhancement of the river gorge incision rate at 11–12 ka (Figure 4b) is thus correlated with the last stage of deglaciation of the Argentera-Mercantour Massif, which also coincides with the important downwasting of Egesen glaciers and a large change in hydrologic conditions [Ivy-Ochs et al., 2008]. The preboreal global-scale warming event resulted in a nearly complete melting of the high-mountain ice cap in the Southern French Alps. Glacier melting and change in hydrologic conditions due to this cold-warm transition period can thus be invoked for this phase of increased incision. Moreover, a switch in sedimentation style from blue clays to organic-rich

## 5. Discussion

As a first approximation, the obtained  $^{36}\text{Cl}$  exposure ages can be interpreted as resulting from a mean incision rate of  $\sim 2.2 \text{ mm a}^{-1}$  over the sampled time period (14 ka), but a more precise analysis of the age/height distribution suggest that important variations can occur at shorter time scales. In any case, incision rate is due to the contribution of both climatic and tectonic (or isostatic) factors. Therefore, estimating the part of tectonic and/or isostatic uplift requires subtracting the shorter-term signals related to changes in climatic-hydrologic conditions. In the following sections, we investigate the effects of climate and of tectonic uplift in the estimated incision rates.

### 5.1. Impact of Glacier Retreat Climatic Fluctuations

Modeled increases in incision rates are dated at 4–5 and 11–12 ka. The oldest incision rate enhancement corresponds to the Preboreal warm period, which followed the Younger Dryas (YD) cold period. The YD corresponds to the last glacier advances in the Alps related to the major cooling event, which led to the deposition of Egesen stadial moraines [e.g., Ivy-Ochs et al., 2008; Böhlert et al., 2011]. Evidences of late Quaternary glaciations (i.e., stadials) are confined to altitudes higher than 1500 m in the Tinée, Vésubie, and Roya valleys. Dubar and Poizat [1976]

sediment is  $^{14}\text{C}$  dated at 11.5 ka from several lakes sequences located in the South Alps [Jorda and de Beaulieu, 1977; Brisset *et al.*, 2013]. The change in lake sediment lithology corresponds to the Holocene climatic optimum, which is recognized in records of alpine lake catchments by soil formation [Ortu *et al.*, 2008; Mourier *et al.*, 2010]. Thus, the development of vegetation could explain the following decrease in incision rate recorded after 11 ka in the studied Vésubie River section.

The increase in incision rates at 4 to 5 ka may also be explained by a climatic factor, corresponding to the middle-late Holocene boundary at 4.2 ka B.P. [Walker *et al.*, 2012]. This boundary corresponds to a period of increased runoff [Walker *et al.*, 2012]. However, several authors have also proposed that changes in sediment content of alpine lakes may reflect anthropic causes [e.g., Brisset *et al.*, 2013]. Agriculture and pastoralism might also have been more important, and the destruction of forests in the water catchment due to this increased land use might have contributed to a larger soil and bedrock erodibility around 4–5 ka [Dubar and Anthony, 1995; Magny *et al.*, 2009; Brisset *et al.*, 2013]. Holocene fluvial sequences in the French Riviera have shown that between 5 and 8 ka B.P., the hydrological regime of rivers was continuously low, whereas the 4–5 ka B.P. period is characterized by more abundant and coarser sediment discharge consistent with a larger incision rate upstream [Dubar and Anthony, 1995]. Finally, Sanchez *et al.* [2010] and Zerathe *et al.* [2013, 2014] have shown that several large-scale landslides were triggered in the southeastern Alps during the 3.3–5.1 ka time period. This coincidence can be regarded as a new evidence of possible intense hydrological pulses in this region during the middle-late Holocene climatic transition.

## 5.2. Long-Term Uplift Rate and Incision Coefficient

The age versus height distribution of sampled points can be satisfactorily reproduced with a power law model of stream incision in which the mean erodibility coefficient  $K$  for the last 16 ka is of  $9 \pm 1 \times 10^{-6} \text{ m}^{-0.475} \text{ a}^{-1}$ , whatever the uplift rate.  $K$  variations over shorter time scales are also constrained independently of the uplift rate. This suggests that measured incision rates are dominated by a climatic signal rather than by the effect of tectonic uplift, at least for the recent period (14–15 ka). By comparing long-term (2 Ma)  $U/K$  couples that fit the river longitudinal profiles and the short-term (16 ka)  $K$  values that reproduce the measured age/height distribution of samples, two interpretations arise: if the long-term uplift rate was significantly lower than the short-term incision rate (i.e., lower than  $2.2 \text{ mm a}^{-1}$ ), then the  $K$  coefficient should have increased during the recent period, due to enhanced water runoff for instance. On the other hand, if one considers that the long-term  $K$  coefficient has not changed during the last 2 Ma, then the long-term uplift rate should be equal to the short-term incision rate (i.e.,  $2.2 \text{ mm a}^{-1}$ ).

Long-term uplift estimates derived from thermochronology [Sanchez *et al.*, 2011] are of about  $0.8\text{--}1 \text{ mm a}^{-1}$  since 22 Ma in the Argentera-Mercantour massif. Uplift rates of  $1\text{--}2 \text{ mm a}^{-1}$  have also been obtained by GPS measurements in the higher parts of Alps, although no data point exists close to our study area [Serpelloni *et al.*, 2013]. Vernant *et al.* [2013] proposed that these rapid uplift rates are due to an isostatic readjustment in response to a recent increase in denudation rates. A similar interpretation from Apatite Fission Tracks / Helium ages is proposed by Valla *et al.* [2011] and Cederbom *et al.* [2011], who documented increased denudation rates since 1 Ma in the Central Alps and 5 Ma at the alpine scale, respectively. In the External Crystalline Massifs, the long-term exhumation rate is of the same order ( $1 \text{ mm a}^{-1}$ ) over a period between 15 and 22 Ma [e.g., Rolland *et al.*, 2008; Sanchez *et al.*, 2011]. Hence, independent data suggest that the long-term uplift rate should be about twice as low as the mean 14 ka incision rate obtained by  $^{36}\text{Cl}$  dating. This in turn suggests that the average  $K$  coefficient has increased during this recent period compared to the longer term (2 Ma) rate. The valley-perpendicular topographic profile has a typical wineglass shape (Figure 2) with a steep inner gorge underlying more gentle hillslopes, which is in agreement with this hypothesis.

In any cases, our models consistently predict satisfying river longitudinal profiles for a constant rock uplift rate, which thus represents the net uplift rate of the onshore continental margin with respect to its offshore oceanic (or thinned continental) counterpart, since sea level variations are taken into account. This result is in agreement with previously published evidences for active uplifting of the North Ligurian margin east of the Var River valley as evidenced by anomalously convex submarine canyons longitudinal profiles [Migeon *et al.*, 2011] and by the tilting and offset of the Messinian erosion surface on the offshore thinned margin [Bigot-Cormier *et al.*, 2004]. Both studies propose that an active reverse fault system located at the foot of the thinned continental margin is responsible for the observed deformations. Comparison with GPS data suggest



that this uplift is at least partly related to the ongoing Africa-Eurasia plate convergence responsible for moderate compressional strain in this area [Calais *et al.*, 2000]. Whatever the long-term rock uplift rate, our study provides evidences of rapid incision of the Mesozoic sedimentary cover of the Vésubie catchment area at a rate of  $2.2 \text{ mm a}^{-1}$  during the late Pleistocene to Holocene period.

## 6. Conclusion

Quantification of river incision rate using in the situ-produced  $^{36}\text{Cl}$  cosmogenic nuclide was successfully performed in a carbonate river gorge dug by the Vésubie River, in the Southern French Alps. The processed samples allows us to decipher incision rate variations with a resolution of about 1 ka during the last 14 ka, and give a mean incision rate for the considered time period of  $2.2 \text{ mm a}^{-1}$ . Modeling of the evolution of the incision in the Vésubie River over 2 Ma based on the stream power law shows that an equilibrium profile compatible with observations can be reached with any long-term uplift rates of  $0.5$  to  $2 \text{ mm a}^{-1}$ , and  $K$  coefficients of  $2.5$  to  $9 \times 10^{-6} \text{ m}^{-0.475} \text{ a}^{-1}$ . However, matching the average age/height distribution of the samples for the last 14 ka requires a significant increase in the  $K$  coefficient (up to  $9 \pm 1 \times 10^{-6} \text{ m}^{-0.475} \text{ a}^{-1}$ ) if the considered long-term uplift rate is significantly lower than the average incision rate of  $2.2 \text{ mm a}^{-1}$ . This is in agreement with the wineglass shape of the valley at this place, suggesting slower incision and perhaps more active hillslope processes prior to 14 ka, followed by enhanced vertical incision. Moreover, the age/height distribution of samples highlights two periods of rapid incision: (i) one at  $\sim 11$ – $12$  ka and (ii) one at  $\sim 4$ – $5$  ka. These periods coincide with changes in climatic conditions characterized by more abundant rainfall and increased runoff.

## Acknowledgments

Constructive reviews by Mikael Attal, Naki Akçar, and an anonymous reviewer, and by Alexander Densmore (Editor) were greatly appreciated. This study has been funded by the French CNRS-INSU SYSTER program and benefited from internal support from the Observatoire de la Côte d'Azur. Marianne Saillard benefited from a 2 month research grant from Geoazur. M. Arnold, G. Aumaître, and K. Keddadouche are thanked for their valuable assistance during  $^{36}\text{Cl}$  measurements at the ASTER AMS national facility (CEREGE, Aix en Provence) which is supported by the INSU/CNRS, the ANR through the "Projets thématiques d'excellence" program for the "Equipements d'excellence" ASTER-CEREGE action, IRD, and CEA. Special thanks to those who bravely crossed the river and climbed the cliff with us to catch the samples (Bruno Scalabrino and Bruno Wilhem) and to Lucie Orsoni who prepared the samples.

## References

- Akaike, H. (1974), A new look at the statistical model identification, *IEEE Trans. Autom. Control*, *19*, 716–723, doi:10.1109/TAC.1974.1100705.
- Akçar, N., P. Deline, S. Ivy-Ochs, V. Alfimov, I. Hadjas, P. W. Kubik, M. Christel, and C. Schlüchter (2012), The 1717 AD rock avalanche deposits in the upper Ferret Valley (Italy): A dating approach with cosmogenic  $^{10}\text{Be}$ , *J. Quat. Sci.*, *27*, 383–392.
- Attal, M., G. E. Tucker, A. C. Whittaker, P. A. Cowie, and G. P. Roberts (2008), Modeling fluvial incision and transient landscape evolution: Influence of dynamic channel adjustment, *J. Geophys. Res.*, *113*, F03013, doi:10.1029/2007JF000893.
- Baotian, P., H. Xiaofei, G. Hongshan, H. Zhenbo, C. Bo, G. Haopeng, and L. Qingyang (2013), Late Quaternary river incision rates and rock uplift pattern of the eastern Qilian Shan Mountain, China, *Geomorphology*, *184*, 84–97, doi:10.1016/j.geomorph.2012.11.020.
- Bauve, V., Y. Rolland, G. Sanchez, G. Giannnerini, D. Schreiber, M. Corsini, J.-L. Perez, and A. Romagny (2012), Pliocene to Quaternary deformation in the Var Basin (Nice, SE France) and its interpretation in terms of "slow-active" faulting, *Swiss J. Geosci.*, *105*, 361–376.
- Bauve, V., R. Plateaux, Y. Rolland, G. Sanchez, N. Bethoux, B. Delouis, and R. Darnault (2014), Long-lasting transcurrent tectonics in SW Alps evidenced by Neogene to present-day stress fields, *Tectonophysics*, *621*, 85–100, doi:10.1016/j.tecto.2014.02.006.
- Benedetti, L., R. Finkel, D. Papanastassiou, G. King, R. Armijo, F. J. Ryerson, D. Farber, and F. Flerit (2002), Post-glacial slip history of the Sparta fault (Greece) determined by  $^{36}\text{Cl}$  cosmogenic dating: Evidence for non-periodic earthquakes, *Geophys. Res. Lett.*, *29*(8), 1246, doi:10.1029/2001GL014510.
- Benedetti, L., R. Finkel, G. King, R. Armijo, D. Papanastassiou, F. J. Ryerson, F. Flerit, D. Farber, and G. Styrakakis (2003), Motion on the Kaparelli fault (Greece) prior to the 1981 earthquake sequence determined from  $^{36}\text{Cl}$  cosmogenic dating, *Terra Nova*, *15*, 118–124.
- Bigot-Cormier, F., F. Sage, M. Sosson, J. Déverchère, M. Ferrandini, P. Guennoc, M. Popoff, and J.-F. Stephan (2004), Déformations pliocènes de la marge Nord-Ligure (France): Les conséquences d'un chevauchement crustal sud-alpin, *Bull. Soc. Geol. Fr.*, *175*, 197–211.
- Böhler, R., M. Egli, M. Maisch, D. Brandová, S. Ivy-Ochs, P. W. Kubik, and W. Haeberli (2011), Application of a combination of dating techniques to reconstruct the late glacial and early Holocene landscape history of the Albula region (eastern Switzerland), *Geomorphology*, *127*, 1–13.
- Braucher, R., S. Merchel, J. Borgomano, and D. L. Bourlès (2011), Production of cosmogenic radionuclides at great depth: A multielement approach, *Earth Planet. Sci. Lett.*, *309*, 1–9.
- Brisset, E., et al. (2013), Non-reversible geosystem destabilisation at 4200 cal. BP: Sedimentological, geochemical and botanical markers of soil erosion recorded in a Mediterranean alpine lake, *Holocene*, *23*, 1863–1874.
- Brocard, G. Y., P. A. van der Beek, D. Bourlès, L. L. Siame, and J.-L. Mugnier (2003), Long-term fluvial incision rates and postglacial river relaxation time in the French Western Alps from  $^{10}\text{Be}$  dating of alluvial terraces with assessment of inheritance, soil development and wind ablation effects, *Earth Planet. Sci. Lett.*, *209*, 197–214.
- Brown, E. T., D. L. Bourlès, G. M. Raisbeck, F. Yiou, B. C. Burchfield, P. Molnar, D. Qidong, and J. Li (1998), Estimation of slip rates in the Southern Tien Shan using cosmic ray exposure dates of abandoned alluvial fans, *Geol. Soc. Am. Bull.*, *110*, 377–386.
- Burbank, D. W., J. Leland, E. Fielding, R. S. Anderson, N. Brozovic, M. R. Reid, and C. Duncan (1996), Bedrock incision, rock uplift and threshold hillslopes in the northwestern Himalayas, *Nature*, *379*, 505–510.
- Calais, E., L. Galisson, J.-F. Stephan, J. Delteil, J. Déverchère, C. Larroque, B. Mercier de Lépinay, M. Popoff, and M. Sosson (2000), Crustal strain in the Southern Alps, France, 1948–1998, *Tectonophysics*, *319*, 1–17.
- Campredon, R., M. Franco, G. Giannnerini, P. Gigot, F. Irr, M. Lanteaume, H. Spini, and J.-F. Tapoul (1977), Les déformations de conglomérats pliocènes de l'arc de Nice (chaînes subalpines méridionales), *C. R. Somm. Soc. Géol. Fr.*, *2*, 75–77.
- Carcaillet, J., I. Manighetti, C. Chauvel, A. Schlagenhauf, and J. M. Nicole (2008), Identifying past earthquakes on an active normal fault (Magnolia, Italy) from the chemical analysis of its exhumed carbonate fault plane, *Earth Planet. Sci. Lett.*, *271*, 145–158, doi:10.1016/j.epsl.2008.03.059.
- Cederbom, C. E., P. van der Beek, F. Schlunegger, H. D. Sinclair, and O. Oncken (2011), Rapid extensive erosion of the North Alpine foreland basin at 5–4 Ma, *Basin Res.*, *23*, 528–550.

- Clauzon, G. (1975), Sur l'âge villafranchien du chevauchement subalpine au droit de Puimoisson (Alpes de Haute-Provence), *C.R. Acad. Sci. Paris*, **280**, 2433–2436.
- Corsini, M., G. Ruffet, and R. Caby (2004), Alpine and late-hercynian geochronological constraints in the Argentera massif (Western Alps), *Eclogae Geol. Helv.*, **97**, 3–15.
- Courboux, F., C. Larroque, A. Deschamps, C. Kohrs-Sansorny, C. Gélis, and J. L. Got (2007), Seismic hazard on the French Riviera: Observations, interpretations and simulations, *Geophys. J. Int.*, **170**, 387–400.
- Daniels, J. M. (2008), Distinguishing allogenic from autogenic causes of bed elevation change in Late Quaternary alluvial stratigraphic records, *Geomorphology*, **101**, 159–171.
- Darnault, R., Y. Rolland, D. Bourlès, R. Braucher, G. Sanchez, M. Revel, and S. Bouissou (2012), Timing of the last deglaciation revealed by receding glaciers at the Alpine-scale: Impact on mountain geomorphology, *Quat. Sci. Rev.*, **31**, 127–142, doi:10.1016/j.quascirev.2011.10.019.
- De Beaulieu, J.-L. (1977), Contribution pollenanalytique à l'histoire tardiglaciaire et Holocène de la végétation des Alpes méridionales françaises, Unpublished thesis, France, Aix-Marseille Université.
- Dubar, M., and E. J. Anthony (1995), Holocene environmental change and river-mouth sedimentation in the Baie des Anges French Riviera, *Quat. Res.*, **43**, 329–343.
- Dubar, M., and M. Poizat. (1976), Le glaciaire de la vallée des Merveilles (Alpes-Maritimes), paper presented at the IXe congrès de l'U.I.S.P.P. Nice, France.
- Dunai, T., and F. M. Stuart (2009), Reporting of cosmogenic nuclide data for exposure age and erosion rate determinations, *Quat. Geochronol.*, **4**, 437–440.
- Federici, P. R., D. E. Granger, A. Ribolini, M. Spagnolo, M. Pappalardo, and A. J. Cyr (2012), Last Glacial Maximum and the Gschnitz stadial in the Maritime Alps according to  $^{10}\text{Be}$  cosmogenic dating, *Boreas*, **41**(2), 277–291, doi:10.1111/j.1502-3885.2011.00233.x.
- Ferrier, K. L., K. L. Huppert, and J. T. Perron (2013), Climatic control of bedrock river incision, *Nature*, **496**, 206–209, doi:10.1038/nature11982.
- Fifield, L. K., T. R. Ophel, G. L. Allan, J. R. Bird, and R. F. Davie (1990), Accelerator mass spectrometry at the Australian National University's 14UD accelerator: Experience and developments, *Nucl. Instrum. Methods Phys. Res., Sect. B*, **52**, 233–237.
- Gosse, J. C., and F. M. Phillips (2001), Terrestrial in situ cosmogenic nuclides: Theory and application, *Quat. Sci. Rev.*, **20**, 1475–1560.
- Ivy-Ochs, S., H. Kerschner, A. Reuther, F. Preusser, K. Heine, M. Maisch, P. W. Kubik, and C. Schlüchter (2008), Chronology of the last glacial cycle in the European Alps, *J. Quat. Sci.*, **23**, 559–573.
- Jorda, M., and J.-L. de Beaulieu (1977), Tardiglaciaire et Postglaciaire des Alpes de Haute-Provence. Le glaciaire de la Blanche, Trois évènements, *Bull. Assoc. Fr. Etud. Quat.*, **14**, 3–15, doi:10.3406/quate.1977.1307.
- Jorda, M., and T. Rosique (1994), Le Tardiglaciaire des Alpes françaises du Sud: Rythme et modalités des changements bio-morphoclimatiques, *Quaternaire*, **5**, 141–149.
- Jorda, M., T. Rosique, and J. Évin (2000), Données nouvelles sur l'âge du dernier maximum glaciaire dans les Alpes méridionales françaises, *C.R. Acad. Sci., Ser. IIA: Earth Planet. Sci.*, **331**, 187–193, doi:10.1016/S1251-8050(00)01408-7.
- Julian, M. (1980), Les Alpes Maritimes Franco-Italiennes: Etude Géomorphologique, Thèse d'Etat Thesis, Aix-Marseille II University, 836 pp.
- Kirby, E., and K. X. Whipple (2012), Expression of active tectonics in erosional landscapes, *J. Struct. Geol.*, **44**, 54–75.
- Lambeck, K., and E. Bard (2000), Sea-level change along the French Mediterranean coast for the past 30000 years, *Earth Planet. Sci. Lett.*, **175**, 203–222.
- Magny, M., B. Vannière, G. Zanchetta, E. Fouache, G. Touchais, L. Petrika, C. Coussot, A.-C. Walter-Simonet, and F. Arnaud (2009), Possible complexity of the climatic event around 4300–3800 cal. B.P. in the central and western Mediterranean, *Holocene*, **19**, 823–833, doi:10.1177/0959683609337360.
- Migeon, S., A. Cattaneo, V. Hassoun, C. Larroque, N. Corradi, F. Fanucci, A. Dano, B. Mercier de Lepinay, F. Sage, and C. Gorini (2011), Morphology, distribution and origin of recent submarine landslides of the Ligurian Margin (North-western Mediterranean): Some insights into geohazard assessment, *Mar. Geophys. Res.*, **32**, 225–243.
- Mourier, B., J. Poulenard, C. Carcaillet, and D. Williamson (2010), Soil evolution and subalpine ecosystem changes in the French Alps inferred from geochemical analysis of lacustrine sediments, *J. Paleolimnol.*, **44**, 571–587, doi:10.1007/s10933-010-9438-0.
- Mudd, S. M., M. Attal, D. T. Milodowski, S. W. D. Grieve, and D. A. Valters (2014), A statistical framework to quantify spatial variation in channel gradients using the integral method of channel profile analysis, *J. Geophys. Res. Earth Surf.*, **119**, 1–15, doi:10.1002/2013JF002981.
- Ortu, E., J.-L. de Beaulieu, and R. Caramiello (2008), Late Glacial and Holocene vegetation dynamics at various altitudes in the Ellero Valley, Maritimes-Alps, northwestern Italy, *Ecoscience*, **15**, 200–212.
- Palumbo, L., L. Benedetti, D. L. Bourlès, A. Cinque, and R. Finkel (2004), Slip history of the Magnolia fault (Apennines. Central Italy) from  $^{36}\text{Cl}$  surface exposure dating: Evidence for strong earthquakes over the Holocene, *Earth Planet. Sci. Lett.*, **225**, 163–176.
- Perron, J. T., and L. Royden (2013), An integral approach to bedrock river profile analysis, *Earth Surf. Processes Landforms*, **38**, 570–576, doi:10.1002/esp.3302.
- Petersen, J., B. Wilhelm, M. Revel, Y. Rolland, C. Crouzet, F. Arnaud, E. Brisset, E. Chaumillon, and O. Magand (2014), Sediments of Lake Vens (SW European Alps, France) record large-magnitude earthquake events, *J. Paleolimnol.*, **51**, 343–355.
- Righter, K., M. Caffee, J. Rosas-Elguera, and V. Valencia (2010), Channel incision in the Rio Atenguillo, Jalisco, Mexico, defined by  $^{36}\text{Cl}$  measurements of bedrock, *Geomorphology*, **120**, 279–292.
- Ritz, J.-F., E. T. Brown, D. L. Bourlès, H. Philip, A. Schlupp, G. M. Raisbeck, F. Yiou, and B. Enkhtuvshin (1995), Slip rates along active faults estimated with cosmic-ray-exposure dates: Application to the Bogd fault Gobi-Altaï Mongolia, *Geology*, **23**, 1019–1022.
- Rolland, Y., M. Rossi, S. F. Cox, M. Corsini, N. Mancktelow, G. Pennacchioni, M. Fornari, and A. M. Boullier (2008),  $^{40}\text{Ar}/^{39}\text{Ar}$  dating of syn-kinematic white mica: Insights from fluid-rock reaction in low-grade shear zones (Mont Blanc Massif) and constraints on timing of deformation in the NW External Alps, in *The Internal Structure of Fault Zones: Implications for Mechanical and Fluid-Flow Properties*, edited by C. A. J. Wibberley et al., Spec. Pub., vol. 299, pp. 293–315, Geol. Soc., London, doi:10.1144/SP299.17.
- Sadier, B., J.-J. Delannoy, L. Benedetti, D. L. Bourlès, S. Jaillet, J.-M. Geneste, A. -E. Lebatard, and M. Arnold (2012), Further constraints on the Chauvet cave artwork elaboration, *Proc. Natl. Acad. Sci. U.S.A.*, **109**, 8002–8006.
- Sage, F., et al. (2011), Structure and evolution of a passive margin in a compressive environment: Example of the south-western Alps-Ligurian basin junction during the Cenozoic, *Mar. Pet. Geol.*, **28**, 1263–1282.
- Sanchez, G., Y. Rolland, M. Corsini, R. Braucher, D. Bourlès, M. Arnold, and G. Aumaitre (2010), Relationships between tectonics, slope instability and climate change: Cosmic ray exposure dating of active faults, landslides and glacial surfaces in the SW Alps, *Geomorphology*, **117**, 1–13.
- Sanchez, G., Y. Rolland, M. Corsini, M. Jolivet, S. Bricaud, and A. Carter (2011), Exhumation controlled by transcurrent tectonics: The Argentera-Mercantour massif (SW Alps), *Terra Nova*, **23**, 116–126.

- Schaller, M., N. Hovius, S. D. Willett, S. Ivy-Ochs, H.-A. Synal, and M.-C. Chen (2005), Fluvial bedrock incision in the active mountain belt of Taiwan from in situ-produced cosmogenic nuclides, *Earth Surf. Processes Landforms*, **30**, 955–971.
- Schimmelpfennig, I., L. Benedetti, R. Finkel, R. Pik, P.-H. Blard, D. Bourlès, P. Burnard, and A. Williams (2009), Source of in situ  $^{36}\text{Cl}$  in basaltic rocks. Implication for calibration of production rates, *Quat. Geochronol.*, **4**, 441–461.
- Schlagenhauf, A., Y. Gaudemer, L. Benedetti, I. Manighetti, L. Palumbo, I. Schimmelpfennig, R. Finkel, and K. Pou (2010), Using in situ Chlorine-36 cosmonuclide to recover past earthquake histories on limestone normal fault scarps: A reappraisal of methodology and interpretations, *Geophys. J. Int.*, **182**, 36–72, doi:10.1111/j.1365-246X.2010.04622.x.
- Serpelloni, E., C. Faccenna, G. Spada, D. Dong, and S. D. P. Williams (2013), Vertical GPS ground motion rates in the Euro-Mediterranean region: New evidence of velocity gradients at different spatial scales along the Nubia-Eurasia plate boundary, *J. Geophys. Res. Solid Earth*, **118**, 6003–6024, doi:10.1002/2013JB010102.
- Sharma, P., P. W. Kubik, U. Fehn, H. E. Gove, K. Nishiizumi, and D. Elmore (1990), Development of  $^{36}\text{Cl}$  standards for AMS, *Nucl. Instrum. Methods Phys. Res., Sect. B*, **52**, 410–415.
- Stock, J. D., and D. R. Montgomery (1999), Geologic constraints on bedrock river incision using the stream power law, *J. Geophys. Res.*, **104**, 4983–4993.
- Stock, J. D., D. R. Montgomery, B. D. Collins, W. E. Dietrich, and L. Sklar (2004), Field measurements of incision rates following bedrock y exposure: Implications for process controls on the long profiles of valleys cut by rivers and debris flows, *Geol. Soc. Am. Bull.*, **117**, 174–194.
- Stone, J. O. (2000), Air pressure and cosmogenic isotope production, *J. Geophys. Res.*, **105**, 23,753–23,759.
- Valla, P. G., P. A. van der Beek, and D. Lague (2010), Fluvial incision into bedrock: Insights from morphometric analysis and numerical modeling of gorges incising glacial hanging valleys (Western Alps, France), *J. Geophys. Res.*, **115**, F01004, doi:10.1029/2008JF001079.
- Valla, P. G., D. L. Shuster, and P. A. Van der Beek (2011), Significant increase in relief of the European Alps during mid-Pleistocene glaciations, *Nat. Geosci.*, **4**, 688–692.
- Van der Woerd, J., F. J. Ryerson, P. Tapponnier, Y. Gaudemer, R. Finkel, A. S. Mériaux, M. Caffee, Z. Guoguang, and H. Qunlu (1998), Holocene left-slip rate determined by cosmogenic surface dating on the Xidatan segment of the Kunlun fault (Qinghai, China), *Geology*, **26**, 695–698.
- Vandenberghe, J. (2003), Climate forcing of fluvial system development: An evolution of ideas, *Quat. Sci. Rev.*, **22**, 2053–2060.
- Vernant, P., F. Hivert, J. Chery, P. Steer, R. Cattin, and A. Rigo (2013), Erosion-induced isostatic rebound triggers extension in low convergent mountain ranges, *Geology*, **41**, 467–470, doi:10.1130/G33942.1.
- Walker, M. J. C., M. Berkelhammer, S. Björck, L. C. Cwynar, D. A. Fisher, A. J. Long, J. J. Lowe, R. M. Newnham, O. Rasmussen, and H. Weiss (2012), Formal subdivision of the Holocene Series/Epoch: A discussion paper by a working group of INTIMATE (Integration of ice-core, marine and terrestrial records) and the Subcommission on Quaternary Stratigraphy (International Commission on Stratigraphy), *J. Quat. Sci.*, **27**, 649–659.
- Whipple, K. X., and G. E. Tucker (1999), Dynamics of the stream-power river incision model: Implications for height limits of mountain ranges, landscape response timescales, and research needs, *J. Geophys. Res.*, **104**, 17,661–17,674.
- Wobus, C., K. X. Whipple, E. Kirby, N. Snyder, J. Johnson, K. Spyropolou, B. Crosby, and D. Sheehan (2006), Tectonics from topography: Procedures, promise, and pitfalls, in *Tectonics, Climate, and Landscape Evolution*, Spec. Paper, vol. 398, edited by S. D. Willett et al., pp. 55–74, Geol. Soc. Am., Penrose Conference Series.
- Zerathe, S., R. Braucher, T. Lebourg, D. Bourlès, M. Manetti, and L. Leanni (2013), Dating chert (diagenetic silica) using in-situ produced  $^{10}\text{Be}$ : Possible complications revealed through the comparison with  $^{36}\text{Cl}$  applied on coexisting limestone, *Quat. Geochronol.*, **17**, 81–93.
- Zerathe, S., T. Lebourg, R. Braucher, and D. Bourlès (2014), Mid-Holocene cluster of large-scale landslides revealed in the Southwestern Alps by  $^{36}\text{Cl}$  dating. Insight on an Alpine-scale landslide activity, *Quat. Sci. Rev.*, **90**, 106–127.